Pt/C catalyst for PEM fuel cells: Control of Pt nanoparticles characteristics through a novel plasma deposition method

Mathilde Laurent-Brocq [a,*], Nathalie Job [b], David Eskenazi [b], Jean-Jacques Pireaux [a]

[a] Laboratoire Interdisciplinaire de Spectroscopie Electronique, Research Centre in Physics of Matter and Radiation (PMR), University of Namur, 61 Rue de Bruxelles, 5000 Namur, Belgium
[b] Laboratoire de Génie Chimique – Génie Catalytique, University of Liège, B6a, 3 allée de la Chimie, 4000 Liège, Belgium

A B S T R A C T

A novel low-temperature plasma method, using Pt acetylacetonate as a precursor, was used for the first time to produce Pt/carbon black catalysts for polymer electrolyte membrane fuel cells. Catalysts were prepared under various plasma conditions and characterized by X-ray diffraction, transmission electron microscopy and X-ray photoelectron spectroscopy. Pt nanoparticles with an average diameter of around 3 nm, which are mainly metallic and quite homogeneously distributed with a Pt loading up to 40 wt%, were successfully formed on carbon black by a 100 W–oxygen plasma treatment. During the plasma treatment, the precursor is thermally decomposed, and some oxidized carbon sites or defects appear at the surface of the carbon black due to interactions with the plasma; these oxidized carbon sites or surface defects probably act as anchoring sites for the nucleation of Pt nanoparticles. The decomposition of the precursor mainly depends on the plasma power whereas the formation of the anchoring sites depends on the stirring of the reactants and on the nature of the plasma gas.

© 2013 Elsevier B.V. All rights reserved.

1. Introduction

Polymer electrolyte membrane fuel cells (PEMFC) are appealing for transportation, stationary and portable applications due to their high conversion efficiency (up to 60%) and their zero pollutant and greenhouse gas emissions [1]. They could also assist in regulating the electrical grid by being fuelled with hydrogen produced from renewable energies. Yet their high cost and short lifetime, compared to gasoline engines, impede their commercial wide-spreading. One of the most costly components of the PEMFC is the catalytic layer of the electrodes, which is usually made of a mix of ionomer (Nafion® in most cases) and Pt/carbon black catalyst. The catalysts present high platinum content (typically 20–80 wt%) to hasten the chemical reactions, especially the sluggish oxygen reduction reaction, while keeping the electrode as thin as possible to avoid mass transport limitations and minimize the ohmic losses caused by proton transport in the ionomer network. However, high Pt loadings in the catalytic layers do not guarantee optimal Pt utilization: in most cases, a large fraction of Pt atoms are not active due to (i) a non-optimal Pt dispersion on the support and (ii) a lack of contact between the supported Pt nanoparticles and the ionomer [2].

According to Gasteiger et al. [3], for automotive applications, Pt-specific densities are required to be lowered down to $0.2\,g_{Pt}/kW$, which corresponds to a maximum loading of the membrane electrode assembly (MEA) of $0.15\,mg_{Pt}/cm2MEA$. This represents a four to six fold reduction of the current MEA loading. Thus one strategy to reduce PEMFC cost is to decrease the platinum loading in the electrodes while maintaining the same catalytic properties by optimizing the platinum utilization. To achieve this goal, the Pt dispersion on the support has first to be optimized from the point of view of the catalytic performances, even for high Pt loadings. Indeed, the catalytic performances strongly depend (i) on the size of Pt nanoparticles (NPs) and (ii) the interparticle distance [4,5]. Regarding the NP size, it has been shown that the Pt specific activity towards the oxygen reduction reaction decreases with the NP size for particle diameter smaller than 10 nm; conversely, the electroactive Pt surface increases when the NP size decreases. Thus the mass activity, which depends on both the specific activity and the metal surface, exhibits a maximum for a NP size of ≈3–4 nm [3]. So the optimum Pt dispersion from the cost and performance point of view is Pt NPs with an average size of ≈3–4 nm and a narrow standard deviation. Regarding the interparticle distance, Watanabe et al. [4] showed that when the intercrystallite distance is greater than an average of 20 nm, the crystallite size effect is not truly dependent on the dimensions of the platinum crystallites but depends on the intercrystallite distance; the interparticle distance itself depends

* Corresponding author. Tel.: +32 081 72 52 32.
E-mail addresses: mathilde.brocq@gmail.com, mathilde.brocq@fundp.ac.be
(M. Laurent-Brocq), Nathalie.job@ulg.ac.be (N. Job), d.eskenazi@ulg.ac.be
(D. Eskenazi), Jean-jacques.pireaux@fundp.ac.be (J.-J. Pireaux).

on the Pt loading and on the support structure. Moreover, NPs need to be free of catalyst poisoning species, such as Cl [6]. Finally, such characteristics of the Pt dispersion should be fulfilled for a large range of Pt mass loading (typically between 20 and 50 wt%). Indeed, since the MEA loading depends not only on the Pt mass loading but also on the thickness and on the density of the electrode, the target MEA loading can be reached through a wide range of Pt mass loadings in the catalyst.

Many routes have been explored up to now for producing Pt/C catalysts [7,8]:

1. The first one is the chemical precipitation, which advantageously proceeds under low temperature conditions. However, especially at high metal loading, the obtained NP size distribution is difficult to control and precipitation often leads to large particle size distributions. This drawback is overcome with impregnation techniques and with the Strong Electrostatic Adsorption method [9,10]. However, for both techniques, depositing a Pt mass loading higher than 25 wt% implies to perform several impregnation-drying-reduction steps in a row, which is time-consuming. Moreover, these methods often use chlorinated metal precursors, and high reduction temperatures are needed to completely remove chlorine that poisons the Pt NPs [9].
2. The use of colloidal suspensions of Pt NPs allows for a very efficient control of NP size [11]. However, colloidal suspensions are expensive and getting rid of the capping agents without inducing a coarsening of the NPs can be difficult.
3. Electrodeposition has been experimented too [12]. But like for the other previously mentioned methods, it is a long and multi-step process.
4. Finally, plasma assisted deposition is an efficient alternative from this last point of view. Indeed, Pt nanoparticles have successfully been anchored onto carbon by physical vapor deposition (PVD) [13] and metal-organic assisted chemical vapor deposition (MO-CVD) has been studied as a valuable depositing process for metallic films, such as Pt [14]. However, in PVD, the substrate is often heated, which is energy-consuming, and high vacuum is needed, which requires complex and expensive pumping devices. In MO-CVD, it is necessary to inject the organometallic in a gaseous state without any decomposition, which is difficult to control and often requires the development of specific precursors.

A novel low temperature radio-frequency plasma deposition method using solid organometallic precursors has been developed to anchor metal or metal oxide nanoparticles onto various powder supports [15]. For example, Pt, Ag and Ni were anchored onto silicon oxide powders, latex beads and multiwall carbon nanotubes, respectively. The method simply consists in applying a short plasma treatment on a solid mixture containing both the organometallic precursor and the nano-powder substrate. No pre- or post-treatment is required, the substrate is not heated, and there is no need to inject a gaseous organometallic precursor. So, this is a "one-pot", fast, easy and low-energy consuming method.

The objective of the present work is to use this new "one-pot" plasma treatment to synthesize Pt/C catalysts with a high Pt weight fraction and that display Pt nanoparticles which are purely metallic, finely dispersed and homogeneously distributed (with an average diameter of 3–4 nm) on the support. Towards this goal, Pt acetylacetonate and carbon black were chosen as the metallic precursor and the carbon support, respectively. Different Pt/C catalysts were synthesized under various conditions (stirring of the reactant mixture during the plasma treatment; plasma power and plasma gas; plasma treatment duration; Pt weight fraction). Then the NPs were characterized by X-Ray diffraction (XRD), transmission electron microscopy (TEM), inductively coupled plasma-atomic
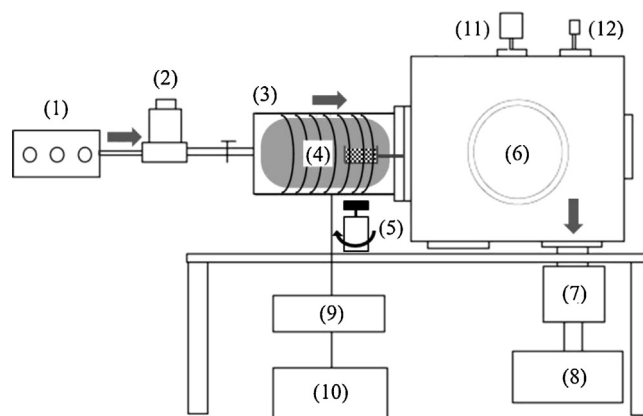

Fig. 1. Scheme of the plasma chamber. (1) Plasma gas inlet, (2) flow rate controller, (3) quartz reactor surrounded by coils, (4) sample in a glass container, (5) magnetic stirrer (the magnet is within the glass container), (6) stainless steel vacuum chamber, (7) turbo pump, (8) primary pump, (9) radio-frequency (RF) matching unit, (10) RF generator (13.56 MHz), (11) Baratron gauge, (12) atmosphere release valve. The dark grey arrows indicate the gas flow direction and the light grey area represents the glow discharge.

emission spectrometry (ICP-AES) and X-ray photoelectron spectroscopy (XPS).

2. Experimental

2.1. Catalyst synthesis

The chosen carbon support was an ENSACO® carbon black powder (TIMCAL Graphite and Carbon). This carbon black is composed of carbon particles with a diameter ranging from 10 to 70 nm aggregated into micron-sized agglomerates. The metallic precursor was a Pt acetylacetonate powder (($C_5H_7O_2$)$_2$Pt, Sigma–Aldrich, 99.99%). The two solid reactants were mixed so as to achieve a Pt/(Pt + carbon black) weight ratio of 20 or 40 wt%. 180 mg of carbon and metallic precursor powder mix was prepared through the following procedure: (i) Pt acetylacetonate (Ptacac) was mixed with 8 mL of acetone and underwent ultrasound-assisted mixing at a power of 185 W for 5 min; (ii) the solid carbon black (CB) powder was added and the Ptacac/CB/acetone slurry underwent 10 additional minutes of ultrasound mixing at a power of 185 W; (iii) finally, the slurry was dried at around 60 °C while being magnetically stirred until reaching complete solvent evaporation. For studying the functionalization of the carbon black surface, the same procedure was used but the reactant only consisted of 180 mg of carbon black.

The plasma treatment was performed in a home-made vacuum chamber using inductively coupled plasma at the radio-frequency of 13.56 MHz (Fig. 1). The glass dish containing the reactant mixture was placed in the chamber so as to be inside the glow discharge contained in a quartz tube. The volume of the reactant mixture was around 0.2 cm × 4 cm × 4 cm. A magnet was placed in the glass dish and was controlled externally from the chamber in order to stir the powder mixture during plasma treatment. The chamber was pumped until reaching about 1 mTorr (0.13 Pa). Then a controlled flow of gas (either dioxygen or argon) was introduced in order to reach a pressure inside the chamber of 0.1 Torr (13.3 Pa). Several catalysts were synthesized with varying plasma conditions: the reactant mixture was possibly stirred during plasma treatment; plasma gas was O_2 or Ar; a power of 30 or 100 W was applied to sustain the plasma discharge; the treatment lasted for 15 or 30 min. All conditions and the corresponding sample codes are summarized in Table 1. Samples are named CB for the plasma treated carbon black, M for the mixture of carbon black and metallic precursor, and C for the catalysts which have been obtained by plasma treatment.

Table 1
List of the studied samples.

Sample name	Pt loading (wt%)	Stirring of reactants?	Plasma gas	Plasma power (W)	Duration (min)
CB-ref	0	Yes	O_2	100	15
CB–Ar–100 W	0	Yes	Ar	100	15
M	20	–	–	–	–
C-ref	20	Yes	O_2	100	15
C-ns	20	No	O_2	100	15
C–O–30 W	20	Yes	O_2	30	15
C–Ar–30 W	20	Yes	Ar	30	15
C–Ar–100 W	20	Yes	Ar	100	15
C–40Pt	40	Yes	O_2	100	15
C–40Pt–30 min	40	Yes	O_2	100	30

Note. Samples are named CB for the plasma treated carbon black, M for the mixture of carbon black and metallic precursor, and C for the catalysts which have been obtained by plasma treatment. The reference conditions are: 20 wt% of Pt and a plasma treatment of oxygen at a power of 100 W during 15 min. The corresponding catalyst is named C-ref. For other samples, one or two conditions are different from those of references and they are noted in the sample name.

The reference conditions are: 20 wt% of Pt and a plasma treatment of oxygen at a power of 100 W during 15 min. The corresponding catalyst is named C-ref. For other samples, one or two conditions are different from those of the references, which are denoted in the sample name. For example, C–40Pt–30 min is a catalyst containing 40 wt% of Pt (not 20 wt% as in the reference conditions), and which underwent a plasma treatment of oxygen at a power of 100 W during 30 min (not 15 min as in the reference conditions).

The sample temperature during plasma treatment was measured via a thermocouple buried inside 180 mg of carbon black powder. To avoid interferences between the glow discharge and the thermocouple, the plasma treatment was applied in the desired conditions during 15 min; then the plasma discharge was switched off while the thermocouple monitor was switched on. Consequently, the measured temperature might be slightly underestimated.

2.2. Characterization techniques

The possible decomposition of the metallic precursor and the formation of the Pt particles were investigated by X-ray diffraction (XRD) with an X'Pert PRO PANalytical device using the Cu-Kα radiation at 0.154 nm wavelength. The Pt nanoparticle size was estimated from the measured full width at half maximum (FWHM) of the (1 1 1) diffraction peak, using Scherrer's formula [16].

To measure the Pt nanoparticle size, catalysts were observed by transmission electron microscopy (TEM) using a Philips Tecnai 10 microscope with an 80 kV accelerating voltage. The samples were dispersed in isopropanol and subsequently deposited onto a TEM copper grid. The size distributions of the metal nanoparticles were obtained in a semi-automated way, as described hereafter. First, a fully automated procedure was used to detect the intensity local minima in the TEM micrographs. Some of the selected objects correspond to isolated metal particles whereas others are overlapping particles. The second category was automatically eliminated by excluding particles with a solidity lower than 0.9 or an elongation higher than 2. Objects with a diameter smaller than 1 nm were also excluded because it was considered to be beyond the detection limit of the microscope. Explanations on this procedure are given in Ref. [9] Due to the noisiness of the images, however, a significant fraction of the remaining selected objects did not correspond to any metal particle. These false positive signals were therefore removed manually. This entire procedure led to measuring a total of around 250 particles for at least 4 different areas for each sample.

To quantify the Pt loading of the Pt/C catalysts obtained after plasma treatment, the Pt content was measured by inductively coupled plasma-atomic emission spectrometry (ICP-AES, Iris advantage Thermo Jarrel Ash). The preparation of the Pt solutions from the catalysts is thoroughly described in [17].

To quantify the functionalization of the carbon black surface and the Pt oxidation state, X-ray photoelectron spectroscopy (XPS) analysis was also performed on each sample. The device used was a K-alpha Thermo Scientific spectrometer (X-ray beam with a spot size of 400 μm, monochromatized Al-Kα line, $h\nu$ = 1486.6 eV). An ultra-low energy electron beam was used to compensate the charging of the samples during analyses. The powder was fixed on the sample holder using double face carbon tape compatible with high vacuum. It was checked that the carbon tape is not detected. For each sample, high resolution spectra were measured at five different points with a pass energy of 50 eV. Reported atomic compositions are averaged values of these five measurements. C 1s spectra were generated at the beginning and at the end of each point measurement procedure to check that no binding energy shift was induced by a varying charging effect.

For the spectrum analysis, the background signal was first subtracted by the Shirley method [18]. The C 1s spectrum was fitted using six components centred at 284.6 ± 0.2 eV, 285.2 ± 0.2 eV, 286.2 ± 0.2 eV, 287.2 ± 0.2 eV, 288.9 ± 0.2 eV and 290.9 ± 0.1 eV, and attributed to sp2 atoms, sp3 atoms, C—O (hydroxyl), C=O (carbonyl) and C=OOH (carboxyl) and π–π* transition, respectively (the last shake-up peak is not shown on the following figures). These peak binding energies are in agreement with [19–21]. Moreover, the full widths at half maximum (FWHM) of the sp2 and sp3 components, on the one hand, and of the C—OH, C=O and COOH components, on the other hand, were constrained to be equal and lower than 2 eV. Finally, the asymmetry parameters of the sp2 component were calibrated on the C 1s spectrum of pristine carbon black so as to get a quantitative agreement between the concentrations of CO groups, measured on the C 1s spectrum, and of oxygen, measured on the O 1s spectrum. It has to be pointed out that the C 1s curve fitting parameters are different from those of pure graphite, determined from data acquired on the same spectrometer. Larsen and Skou [22] extensively characterized carbon black powders by XPS and underlined the difficulty of the C 1s spectra curve fitting into individual components due to the signal asymmetry and to the low O content.

The Pt 4f spectra were fitted using three spin-orbit coupling doublets (7/2 and 5/2) whose intensity ratio and binding energy difference were held constant at 0.75 and 3.3 ± 0.1 eV respectively. The binding energies of the 7/2 components were centred at 71.3 ± 0.3 eV, 73.0 ± 0.3 eV and 74.9 ± 0.3 eV and were attributed to Pt^0 (metallic), Pt^{2+} (PtO) and Pt^{4+} (PtO_2) respectively, in agreement with previous works [23,24]. Moreover, the FWHM of the Pt^{2+} and Pt^{4+} core level peaks were constrained to be equal. The asymmetry parameters of the metallic doublet were fitted on the XPS data recorded from a state-of-the art commercial Pt/C catalyst (70 wt% Pt loading) supplied by Paxitech whose Pt nanoparticles have a diameter of 3 nm following TEM observations (not presented here), and on a colloidal solution of 3 nm Pt nanoparticles supplied by PlasmaChem: identical asymmetry parameters were determined

in both reference samples. Those asymmetry parameters as well as the peak binding energy are different from those of pure bulk Pt due to a well-documented size-effect (see Section 4 for more details).

The thermal stability of the metallic precursor was investigated by differential scanning calorimetry coupled with differential thermal gravimetry (DSC-DTG) under Ar and O_2 atmosphere, using a Setaram TG-DSC 111 analyzer. Samples of approximately 20 mg were loaded in 100 µL open aluminium crucibles suspended with platinum wires. The analyzer was purged at a 200 mL/min flow rate with Argon (Air Liquide, Alphagaz 1) and oxygen (Air Liquide, N48) respectively. The flow rate was then reduced to 15 mL/min and the samples were subsequently heated at a constant rate of 5 °C/min from room temperature to 500 °C. An empty alumina crucible, similar to the one containing the sample was used as a reference.

3. Results

3.1. Functionalization of carbon black surface by plasma treatment

As a first step of the analysis, the carbon black powder was treated alone for a duration of 15 min within an oxygen plasma in varying conditions (with or without stirring of the powder mixture during the treatment; plasma power ranging between 10 and 100 W; gas pressure ranging between 0.01 and 1 Torr); argon plasma was also used with a power of 100 W, a gas pressure of 0.1 Torr and stirring of the reactants during the treatment. All treated samples were subsequently characterized by XPS.

The carbon black sample treated without stirring of reactants exhibits similar C 1s spectra as the pristine carbon black (Fig. 2a). On the other hand, when reactants are stirred, the C 1s spectrum evolves, as can be seen for example after an O–100 W plasma treatment at 0.1 Torr (Fig. 2b). This is due to the oxidation of carbon at the surface of the carbon black particles, which produces C—O, C=O and C=OO functions. For the tested conditions, the fraction of surface C atoms bonded to O atoms (sums of the C—O, C=O and C=OO C 1s components) ranges from $8 \pm 4\%$ to $15 \pm 4\%$; these values must be compared with that obtained for the pristine carbon black (2% of C atoms bonded to O). No clear relationship between the amount of surface functions and either the plasma power or the gas pressure can be drawn from these results. The carbon black powder treated by Ar plasma exhibits only $3 \pm 2\%$ of surface functionalization (Fig. 2c), which is slightly higher than in the pristine carbon black. Those oxygenated functions are possibly formed (i) during the plasma treatment due to residual O in the chamber or (ii) when the sample is taken out of the reactor. In the latter case, the oxidation would be due to the interaction between air and the surface defects formed by the plasma. Thus, when reactants are stirred, oxygen plasma highly functionalizes the carbon surface; Ar plasma induces minor oxidation only.

3.2. Thermal analysis of Pt acetylacetonate

The thermal stability of the metallic precursor under O_2 or Ar atmosphere was investigated up to 500 °C by differential thermal gravimetry (DTG). In Fig. 3, one can observe that Pt acetylacetonate undergoes a mass loss of 50.1 and 53.5% under O_2 and Ar atmosphere respectively. Since the ligand represents 49.6 wt% of Pt acetylacetonate, the mass loss is likely due to the release of the organic part from Pt. The mass loss takes place mainly between 160 and 210 °C for O_2 and between 190 and 260 °C for Ar. The residues of DTG experiments interrupted after the mass loss (250 and 270 °C under O_2 and Ar atmosphere respectively) were analyzed by XPS. After DTG under O_2, Pt is exclusively in a metal state. So the mass loss can be attributed to the complete release of the organic part
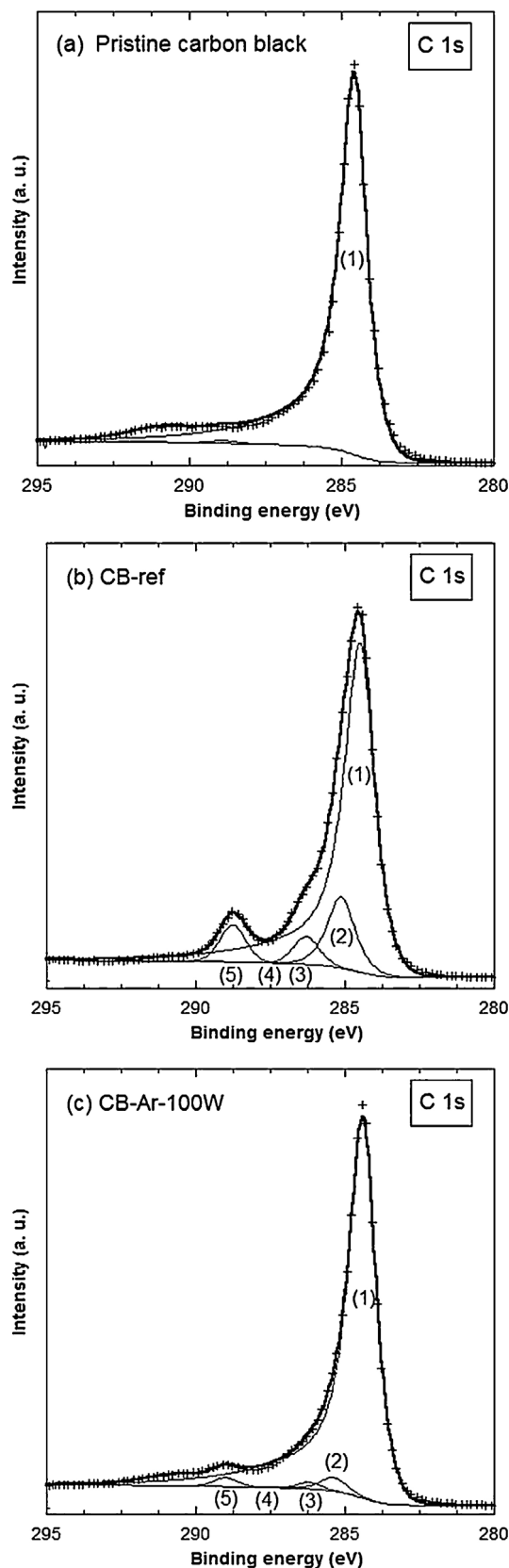

Fig. 2. XPS carbon spectra of (a) pristine carbon black and of carbon black after (b) oxygen or (c) argon plasma treatment at 100 W (black cross). The experimental curve is fitted with five peaks which correspond to: (1) sp2, (2) sp3, (3) C—O, (4) C=O, (5) C=OO. Their sum is also plotted (bold black line).
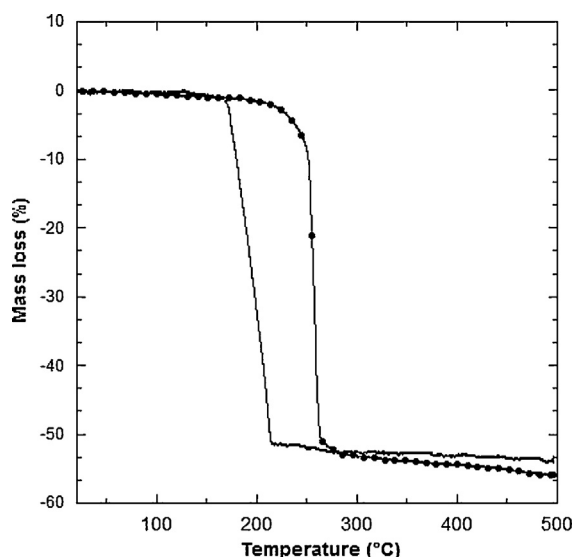
Fig. 3. Differential gravimetric analysis (DTG) of the Pt acetylacetonate powder under O_2 (–) or Ar (●) atmosphere. The mass loss corresponds to the release of the organic ligand.

from Pt. After DTG under Ar, 7 at.% of the total amount of Pt is in an oxidized state. Consequently the decomposition of Ptacac was not total and a part of the mass loss, corresponding to around 12 wt% of the initial mass of Ptacac, is likely to be due to its evaporation.

So the decomposition of Pt acetylacetonate under an oxidative atmosphere such as O_2 is initiated at a lower temperature than under an Ar atmosphere. Afterwards, since the decomposition, which is a combustion, is exothermic (results not shown here), less energy needs to be provided by the plasma to sustain the reaction. Moreover, under an O_2 atmosphere, the thermal decomposition is complete whereas under an Ar atmosphere, some Ptacac remains.

This can interestingly be compared with the temperature of the sample powder during the plasma treatment. Temperatures of 110 °C, 120 °C and 200 °C were measured for 30 W–Ar plasma, 30 W–O plasma and 100 W–O or Ar plasma respectively. It is underlined that this temperature increase of the sample is not due to any additional heating device. If one assumes that the thermal stability of Pt acetylacetonate is similar in the plasma reactor (at low pressure) as in the DTG experiment (at atmospheric pressure), one can infer that the metallic precursor could be thermally decomposed by a 100 W plasma but not by a 30 W plasma. Moreover, if one assumes that the decomposition of Pt acetylacetonate in an O–plasma (at low pressure) is in fact a combustion releasing a significant amount of energy, the decomposition by an 100 W–O plasma might be faster compared to a 100 W–Ar plasma.

3.3. Catalyst synthesis with or without stirring of the reactants

Pt/C catalysts with a 20 wt% Pt loading were produced via a 100 W–O plasma for 15 min, without or with stirring of the reactant powders during the treatment (samples C-ns and C-ref, respectively). Fig. 4a shows the XRD diffractograms of these two samples, as well as that of the untreated reactant mixture (M). The latter exhibits many diffraction peaks around $2\theta = 18°$ and $25°$ which are characteristic of Pt acetylacetonate. Those peaks are absent from the C-ns and C-ref samples. Instead, three new peaks appear at $2\theta = 39.8°$, $46.2°$ and $67.5°$, which correspond to the (1 1 1), (2 0 0) and (2 2 0) planes of the cubic Pt phase [25]. The very broad peak around $25°$ is attributed to carbon black. So, the 100 W–O plasma treatment leads to the decomposition of the metallic precursor without or with stirring of reactants. Since amorphous compounds

or crystallized compounds with very low concentration are not detected by XRD, one cannot exclude the decomposition to be not fully complete. The 100 W–O plasma treatment also leads to the formation of metallic Pt particles. However, the Pt diffraction peaks of the C-ref sample appear to be much broader than those of the C-ns catalyst. Fig. 4b presents a zoom in on the main Pt peak; the average size of the Pt particles, calculated with the Scherrer formula, equals 4.8 nm for the C-ref sample whereas two populations with average sizes of 4.6 and 15.7 nm are needed to adjust the diffraction peak of the C-ns sample (Table 2).

TEM pictures provide evidences that the nanoparticles deposited on the carbon black powder are well dispersed and very densely distributed for both catalysts (Fig. 5a and c). However their spatial distribution differs. Indeed many areas of the C-ns sample are completely free of nanoparticles (Fig. 5b), which is not the case for the C-ref sample. Average particle diameters of 3.3 ± 1.0 nm and 2.7 ± 0.8 nm were measured from the TEM pictures for C-ns and C-ref samples, respectively (d_{TEM} in Table 2). To compare TEM and XRD results, first, it must be considered that TEM permits the measurement of the particle size whereas XRD permits the calculation of the crystallite size. Here, since particles are only a few nanometers large and since the size measured by XRD is not smaller than the one measured by TEM, it is reasonable to assume that particles are monocrystalline, allowing the comparison between TEM and XRD results. Second, since XRD is sensitive to the volume of the particles, a volume weighted average diameter, $d_v = \sum(n_i d_i^4)/\sum(n_i d_i^3)$, was calculated from the particle size distributions obtained from TEM pictures (d_v, Table 2) [26]. d_v matches well the average diameter calculated from XRD diffractograms (d_{XRD}, Table 2) for C-ref and for the smaller particle population for C-ns. The larger Pt particles detected by XRD in the C-ns sample ($d_{XRD} = 15.7$ nm) are not observed by TEM. This is most probably because they are not densely dispersed onto the support. Moreover, since carbon black grains have a similar diameter, it would be difficult to distinguish them from the large Pt particles, especially if carbon grains are on top of each other, making them appear as dark as Pt. To summarize, a 15 min treatment with a 100 W–O plasma leads to the decomposition of the metallic precursor and to the formation of Pt particles without or with stirring of reactants during the treatment. In the first case, (C-ns), small (4.6 nm) and larger (15.7 nm) particles are formed and their spatial distribution is very heterogeneous; in the latter case (C-ref), the Pt particle size distribution is narrow and the NPs are homogeneously distributed over the carbon surface. Given those results, the other studied samples have been produced with stirring of the reactants during the plasma treatment.

3.4. Catalyst synthesis with different plasma gas and power

Plasma produced with O_2 or Ar gas at a power of 30 or 100 W were tested for the synthesis of catalysts (treatment duration = 15 min, Pt loading = 20 wt%, stirred reactants). The corresponding samples are named C–O–30 W, C–Ar–30 W, C-ref (O, 100 W) and C–Ar–100 W. According to the XRD diffractograms (Fig. 4a), Pt acetylacetonate is decomposed by a 100 W–O plasma but not by a 30 W one, either under O or Ar. Moreover, the peaks corresponding to the cubic Pt phase appear only after a plasma treatment of 100 W. The diffractogram of the C–Ar–100 W sample exhibits a minor peak at around 18°, which is characteristic of Pt acetylacetonate, and peaks of the cubic Pt phase, which are slightly less intense than those of the C-ref sample. This result indicates that the Pt acetylacetonate decomposition is not complete in the case of a 15 min Ar plasma treatment. This can be qualitatively explained by the thermal analysis, although it was performed under a tremendously higher pressure than in the plasma chamber (Section 3.2). It was indeed shown that the Pt acetylacetonate decomposition
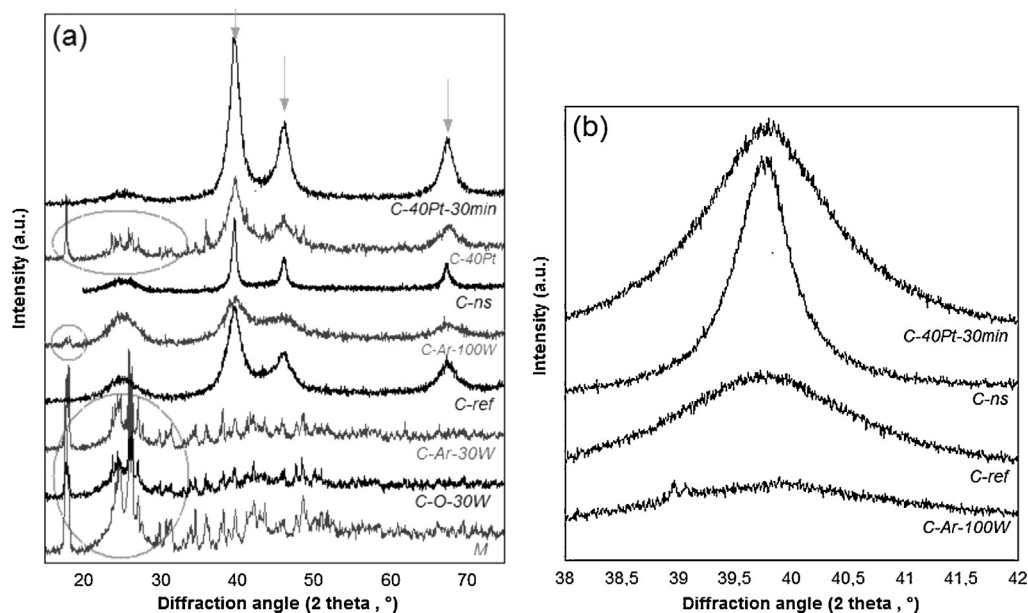
Fig. 4. (a) XRD diffractograms of the mixture of reactants before plasma treatment (M) and of the catalysts obtained under various plasma treatment conditions (C–O–30 W, C–Ar–30 W, C-ref, C–Ar–100 W, C-ns, C–40Pt and C–40Pt–30 min). Grey circles indicate the main diffraction peaks of Pt acetylacetonate while the grey arrows point out the diffraction peaks of the metallic Pt phase. (b) XRD diffractograms focused on the main diffraction peak of metallic Pt for catalysts containing Pt nanoparticles after plasma treatment (C–Ar–100 W, C-ref, C-ns and C–40Pt–30 min).

under O_2 was initiated at a lower temperature and then required less thermal energy to be sustained than decomposition under Ar.

TEM pictures confirm that nanoparticles have been formed only by 100 W plasma syntheses: no nanoparticles are observed for C–O–30 W (Fig. 5d) and C–Ar–30 W samples (similar images as C–O–30 W, no presented here) whereas fine nanoparticles appear to be deposited on carbon black for C-ref (Fig. 5c) and C–Ar–100 W (Fig. 5e). The size of the Pt nanoparticles can be determined both from XRD and TEM analyses (values of d_{XRD} and d_{TEM} in Table 2). From TEM pictures, the C-ref and C–Ar–100 W samples show average diameters of 2.7 and 2.5 nm, respectively, with a standard deviation of 0.8 nm; this is quite adequate for the PEMFC application. Diameters of 4.8 and 3.7 nm are calculated from the XRD diffractograms. They match well the volume weighted average diameter, d_v, calculated from the particle size distributions obtained from TEM pictures. This asserts that the TEM pictures are representative of the whole catalyst and that no larger particles exist, as it was the case for the C-ns sample.

According to ICP-AES results (Table 2), the C-ref and C–Ar–100 W samples exhibit Pt loading of 14.6 and 13.3 wt% respectively, which corresponds to yields of 73 and 67%. The Pt loss

could be due to partial evaporation of Ptacac during the plasma treatment.

XPS analyses give more insights in the chemistry of the catalysts.

- The carbon black surface is significantly more functionalized by the oxygen plasma than by the argon one. Indeed, the functionalization percentage (amount of C surface atoms which are bonded to O atoms) is 11 ± 5.5 and $8 \pm 1.8\%$ for C–O–30 W and C-ref, respectively, whereas it equals 6 ± 1.7 and 4 ± 1.3 for C–Ar–30 W and C–Ar–100 W, respectively (Table 2). No significant effect of the plasma power is observed for the tested range of power. Since similar surface functionalization was observed for carbon black treated alone (see Section 3.1), this asserts that the functionalization is induced by the oxygen plasma and not by interactions with residues of Pt acetylacetonate, whose ligands contain oxygen.
- Fig. 6a and b shows that the Pt 4f spectra recorded for the C–O–30 W and C–Ar–30 W samples are very similar to that of Pt acetylacetonate, confirming the presence of Pt acetylacetonate detected by XRD. More precisely, XPS spectra show that Pt has been partially reduced. So Pt acetylacetonate was altered, although not decomposed, by the plasma treatment.

Table 2
Results of the characterization of the catalysts by XRD, TEM, XPS and ICP.

Sample name	XRD	TEM			XPS		ICP
	d_{XRD} (nm)	d_{TEM} (nm)	σ (nm)	d_v (nm)	CO/C$_{total}$ (%)	PtO$_x$/Pt$_{total}$ (%)	Pt (wt%)
C-ns	4.6–15.7	3.3	1.0	4.5	15 ± 0.6	5 ± 3.6	–[d]
C–O–30 W	–[a]	–[a]	–[a]	–[a]	11 ± 5.5	–[b]	–[a]
C-ref	4.8	2.7	0.8	3.3	8 ± 1.8	11 ± 0.8	14.6
C–Ar–30 W	–[a]	–[a]	–[a]	–[a]	6 ± 1.7	–[b]	–[a]
C–Ar–100 W	3.7	2.5	0.8	3.9	4 ± 1.3	20 ± 5.8[c]	13.3
C–40Pt–30 min	6.7	3.4	0.9	4.1	8 ± 2.6	8 ± 1.5	30.2

d_{XRD} is the average size of Pt particles estimated from XRD peak broadening (Scherrer formula); d_{TEM} is the average size estimated from TEM; σ is the standard deviation associated with d_{TEM}; d_v is the mean volume diameter of Pt particles, $\sum n_i d_i^4 / \sum n_i d_i^3$, estimated from TEM. CO/C$_{total}$ and PtO$_x$/Pt$_{total}$ are ratios of C (respectively Pt) atoms bonded to O atoms to the total amount of C (respectively Pt) calculated from the fitting of XPS spectra.

  a Not relevant: no Pt nanoparticles in these samples.
  b Not relevant: in these samples, Pt acetylacetonate remains and is partly decomposed. Thus Pt in an oxidized state cannot be attributed to nanoparticle surface oxidation.
  c Pt acetylacetonate is not completely decomposed. Thus Pt in an oxidized state is attributed both to nanoparticle surface oxidation and remaining Pt acetylacetonate.
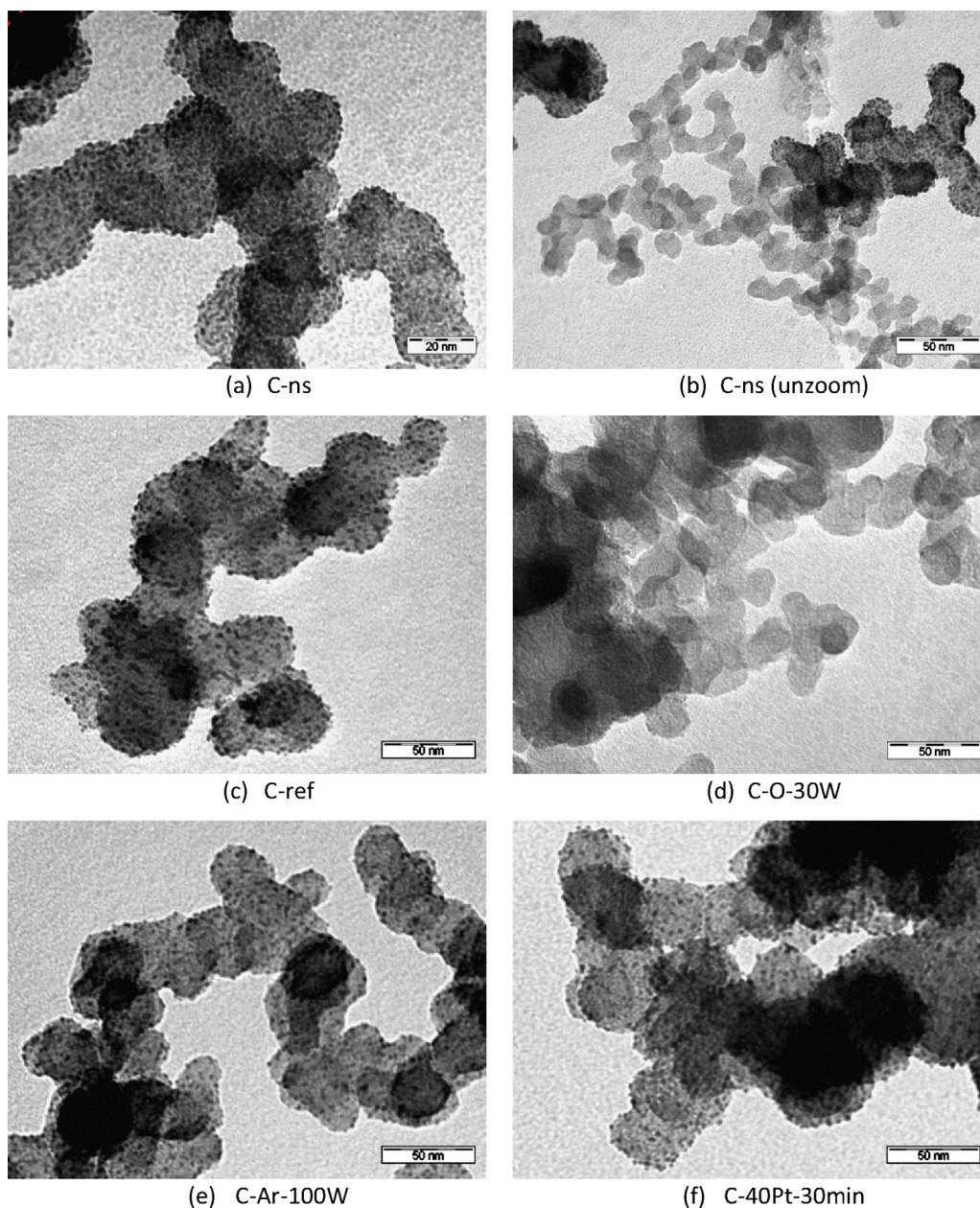 d Not relevant: Pt dispersion does not fill the requirements.

Fig. 5. TEM pictures of the catalysts obtained with plasma treatment under various conditions. One exhibits no nanoparticles ((d) C–O–30 W); another exhibits a fine but heterogeneous dispersion of nanoparticles ((a) and (b), C-ns); the others exhibit a fine and dense dispersion of nanoparticles ((c) C-ref, (e) C–Ar–100 W and (f) C–40Pt–30 min.

- The Pt 4f spectra of the C-ref (Fig. 6c) and C–Ar–100 W (Fig. 6d) samples are fitted with three doublets attributed to Pt^0, Pt^{2+} and Pt^{4+}. For C-ref sample, the Pt^{2+} and Pt^{4+} components represent 11% of the total amount of Pt (Table 2). Since no Pt acetylacetonate was detected in the XRD diffractogram of this sample, Pt^{2+} and Pt^{4+} components are attributed to surface oxidation of the nanoparticles, suggesting that the Pt nanoparticles are mainly metallic. The C–Ar–100 W sample has Pt^{2+} and Pt^{4+} components representing 20% of the total Pt (Table 2). According to the XRD diffractogram (Fig. 4a), there is a little remaining Pt acetylacetonate in this sample. Thus Pt^{2+} and Pt^{4+} components are attributed to remaining Pt acetylacetonate and possible surface oxidation of the Pt nanoparticles.
- Standard deviations of all XPS measurements, which are computed from the data obtained on five analysis points, are large. As an example, the average Pt concentration for C–O–30 W, C-ref,

C–Ar–30 W and C–Ar–100 W, is 3.2 ± 0.9 at.%. This reflects some spatial heterogeneity of the catalyst at the micrometre scale.

To conclude, the 100 W–O plasma treatment appears to be the best conditions among those tested. Indeed, it allows the formation of very well dispersed ($d_{TEM} \approx 3$ nm) and mainly metallic Pt nanoparticles, as required for the PEMFC application.

3.5. Synthesis of catalyst with an increased Pt mass loading

Pt/C catalysts with 40 wt% Pt loading were produced via a 100 W–O plasma with stirring of the reactant powders for 15 and 30 min (named C–40Pt and C–40Pt–30 min respectively). According to the XRD diffractograms (Fig. 4a), peaks characteristic of both Pt acetylacetonate and the metallic Pt phase are present after 15 min of treatment. After 30 min, only the peaks of the metallic
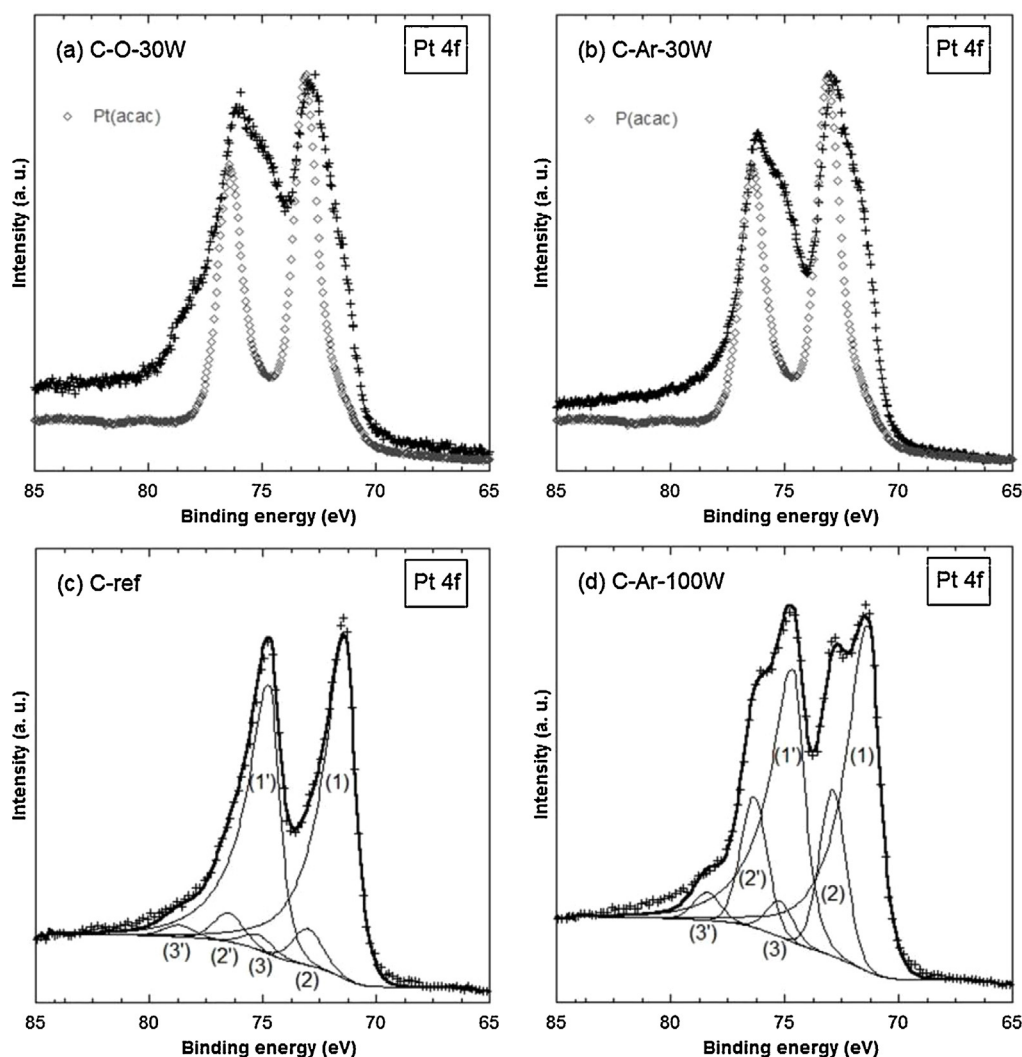
Fig. 6. XPS platinum spectra of the catalysts obtained after oxygen or argon plasma treatment at 30 or 100 W (black cross). For (a) C–O–30 W and (b) C–Ar–30 W, as a comparison, the spectrum of Pt acetylacetonate is superimposed (hollow lozenge). For (c) C-ref and (d) C–Ar–100 W, the experimental curve is fitted with three peak doublets which correspond to: (1) and (1′) Pt^0, (2) and (2′) Pt^{2+} and (3) and (3′) Pt^{4+}. The sum of those doublets is also plotted (bold black line).

Pt phase remain. Thus a higher Pt loading requires a longer plasma treatment for the metallic precursor to be completely decomposed. On the TEM images (Fig. 5f), one can observe that the Pt dispersion of sample C–40Pt–30 min is similar to that of the other catalysts. So, increasing the Pt loading does not lead to a coarsening of the nanoparticles. The average particle size was calculated equal to 3.4 ± 0.9 nm from TEM images. One may note that the XRD diameter is somewhat larger ($d_{XRD} = 6.7$ nm) than the value obtained from TEM ($d_v = 4.1$ nm). This suggests that there are probably some larger nanoparticles. Indeed, if for example 0.5% of particles with a diameter of 15 nm are added to the size distribution measured by TEM, the calculated d_v corresponds to d_{XRD}. This would represent only 1 particle of the total number of particles measured by TEM, which is too few to be easily detected. The recorded XPS spectra are similar to those obtained for the C-ref sample (not shown): 8% of C is functionalized and 8% of Pt is oxidized (Table 2).

A total load of Pt of 30.2 wt% has been quantified by ICP in C–40Pt–30 min (40 wt% theoretical load), to be compared with a load of 14.6 wt% in C-ref (20 wt% theoretical load). The Pt deposition yields are equivalent for both samples (75 and 73% for C–40Pt–30 min and C-ref respectively). So, increasing the amount of metallic precursor does result in increasing the Pt concentration in the catalyst.

4. Discussion

Pt/C catalysts have been synthesized through a plasma treatment of a solid mixture composed of a metallic precursor and a carbon black powder under various conditions and analyzed by different spectroscopic and morphologic tools. From the results obtained, several phenomena taking place during the plasma treatment can be identified.

According to the thermal analysis (Section 3.2), at atmospheric pressure, Pt acetylacetonate, the metallic precursor, is decomposed at a temperature higher than 160 °C and this decomposition is promoted by an O_2 atmosphere compared to an Ar one. Such a sample temperature is reached in a 100 W plasma but not during a 30 W treatment: 100 W power is necessary. XRD results confirm that: (i) Pt acetylacetonate is decomposed in a 100 W plasma but not in a 30 W treatment and that (ii) an oxygen plasma hastens the decomposition compared to an argon one (Section 3.4). Compared to the conditions of the thermal analysis, the oxygen or argon pressure is significantly lower during the plasma treatment, which could reduce the impact of the gas nature on the decomposition. Moreover the plasma could enhance the decomposition, through surface interactions between the powder and the plasma species. For this to occur, stirring of the reactants is

required to allow every powder grain of the reactant mixture to face the plasma at a time during the treatment. Otherwise, since the reactant mixture is 0.2 cm thick, only powder grains on the top might undergo surface interactions with the plasma species. However, in the catalyst produced by a 100 W–O plasma treatment without stirring of reactants, no remaining Pt acetylacetonate is detected (Section 3.3). Consequently, surface interactions between the plasma species and the Pt acetylacetonate do not have a predominant effect on the decomposition of the metallic precursor. The decomposition is mainly attributed to a thermal and chemical effect.

The oxygen plasma treatment leads to the formation of oxidized carbon sites at the surface of the carbon black powder (Section 3.1). It was observed that stirring of the reactants during the plasma treatment is required to oxidize homogeneously the carbon surface. Indeed, as already mentioned, without stirring, only carbon black grains on the top of the reactant mixture can undergo surface interactions with oxygen plasma species. Since the volume of the reactant mixture is around 0.2 cm × 4 cm × 4 cm, most of carbon black grains would remain unoxidized. In a catalyst produced by a 100 W–O plasma without stirring of reactants, which thus contains fewer oxidized carbon sites, the dispersion of nanoparticles is coarser and more heterogeneous than in a catalyst produced in the same conditions but with stirring of the reactants. So, oxidized carbon sites appear to act as anchoring sites for the formation of Pt nanoparticles. A catalyst produced by a 100 W–Ar plasma with stirring of reactants also contains a fine, dense and homogeneous distribution of NPs although much fewer oxidized carbon sites have been obtained by such a plasma treatment (Section 3.1). But one knows that the ions of a plasma are able to produce structural defects and even sputter some atoms when interacting with a surface. Ar plasmas are commonly used for this property in plasma etching applications [27]. Thus the structural surface defects due to the interactions between the carbon black surface and the Ar plasma excited species can be proposed as alternative anchoring sites for the NPs growth. Such structural defects are likely to be also formed, by an oxygen plasma. Finally, when the Pt mass loading is increased, the nanoparticles remain finely dispersed (Section 3.5); this suggests that the anchoring sites are numerous enough to prevent nanoparticle coarsening.

A mechanism for the formation of the Pt nanoparticles on the carbon black powder during the plasma treatment can be proposed (Fig. 7): (i) the metallic precursor is decomposed in the plasma discharge mainly because of thermal and chemical effects, (ii) while interactions of the plasma species with the carbon black surface leads to the appearance of chemical defects (oxygen surface groups) and structural defects; then (iii) Pt nanoparticles nucleate on these defects, which act as anchoring sites. The decomposition of the precursor depends on the plasma power and of the nature of the plasma gas whereas the formation of anchoring sites depends on the stirring of the reactants and of the nature of the plasma gas. From this "one-pot" deposition process, one cannot determine whether those three steps take place simultaneously or one after another. As a comparison, Hermans et al. [28,29] produced a Pd/C catalyst through a sequence of three separate reactions: (i) an acid treatment of carbon black to induce the formation of oxygenated surface functions, (ii) the addition of a metallic precursor that grafted onto the oxygenated sites and (iii) a thermal treatment to decompose the metallic precursor and induce the nucleation of Pd nanoparticles. In this process, step-by-step characterization was possible and thus a very precise mechanism was determined. Our results would be compatible with a mechanism in which the plasma treatment induces defects, and at least part of the metallic precursor molecules are anchored before being decomposed.

The present work shows that stirring of the reactants during the plasma treatment is necessary to obtain finely dispersed and homogeneously distributed Pt nanoparticles on a carbon black nanopowder. However, one must admit that the Pt concentration and the amount of functionalized carbon sites determined by XPS still vary greatly from one point of measurement to another and that some aggregates of carbon black powder without any nanoparticles can still be found by TEM. So there is room for improvement of homogeneity on a micrometre scale.

It was shown that this novel low-temperature plasma method is very efficient for depositing well-dispersed Pt nanoparticles. To decrease the amount of used Pt in the catalyst, it is also of importance to limit Pt loss during the process. This is why the yield of the process was calculated. For the best deposition conditions, that is a 100 W–oxygen plasma with stirring of the reactants during the plasma treatment, a yield of around 75% is reached. For further process development, it is clear that the origin of the Pt losses should be assessed more clearly, and the manufacture method should be optimized so as to reach higher yields. Nevertheless, these first results are promising, first because the Pt losses are relatively low, and second because of the quickness of the method. To compare, it can be reminded that obtaining 15.0 wt% catalyst loading with the strong electrostatic adsorption technique [9] requires two successive impregnation-drying reduction steps, which is quite time-consuming, and uses huge amounts of Pt precursor solution, reaching a yield of about 15% per impregnation run.

The Pt nanoparticles chemical state (metal or oxide) was determined by XPS. This quantification essentially depends on the binding energy and the shape of the Pt^0 peak, which has been thoroughly observed to be size dependent [30–32]. In our experiment, a shift to higher binding energy compared to bulk platinum of around 0.25 eV has been measured. As a consequence, bulk metallic Pt was not chosen as a reference sample; instead, the measurements are compared to (i) a colloidal solution of Pt nanoparticles and (ii) a state-of-the art Pt/carbon black catalyst, which both display Pt nanoparticles with size similar to that observed in our samples. It was assumed that the Pt nanoparticles of the reference samples are free of surface oxidation. However a slight oxidation of those nanoparticles cannot be excluded. Indeed the corresponding peaks on the XPS spectrum would be convoluted with the ones of the metal state. Thus, the Pt oxidation presented here might have been slightly underestimated.

Wertheim et al. [33,34] explained the size-dependency of the shape of metal XPS spectra by a final state effect: the metal cluster is positively charged in the final photoemission state, during the emission of the photoelectron; due to a less efficient charge relaxation in the NPs, a Coulomb attraction between the charged metal cluster and the just-emitted photoelectron decreases the kinetic energy of the last one, which results in an apparent higher binding energy. For the specific case of Pt deposited on graphite, Marcus and Hinnen [32] ascribe the size-dependency of the Pt 4f core level peak to a Pt-support interaction. Going further, Chen et al. [35] and Zhang et al. [36] fitted metal nanoparticles spectra only with symmetric doublets, which enables them to detect a nanoparticle-support interaction for Pd deposited on graphite and an oxidation of the nanoparticle extreme surface for Pt deposited on graphite [35,36]. Thus, the fitting procedure chosen in the present study (Section 2.2) is likely to prevent us from any detection of the Pt nanoparticles-carbon black interaction. Still the approach followed by Chen et al. [35] and Zhang et al. [36] implies to correlate the spectra of the metal, of the support and of oxygen, which would probably be more complex for carbon black than for graphite.

In the near future, new procedures for the mixing of reactants before their introduction inside the plasma chamber and for their stirring during the plasma treatment will be tested so as to improve the homogeneity of the Pt nanoparticles distribution
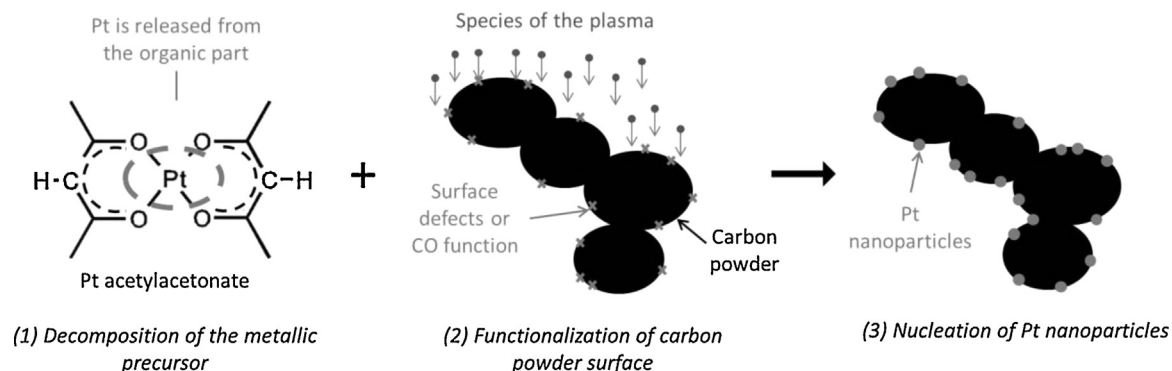
Fig. 7. Mechanism of formation of Pt nanoparticles during the plasma treatment of a metallic precursor (Pt acetylacetonate) mixed with a carbon black powder.

and the process yield. The method will also be applied to deposit Pt nanoparticles on carbon xerogels which are more promising supports for the PEMFC applications [9,10]. The catalysts presenting interesting features in terms of Pt dispersion will also be electro-chemically characterized via CO stripping and oxygen reduction reaction in a three-electrode cell, and then tested as materials for membrane-electrode assemblies of PEM fuel cells. This will give more insight into the importance of the different physicochemi-cal characteristics of the catalyst with regard to the electrocatalytic properties, like a possible surface oxidation of Pt NPs and/or car-bon black or heterogeneity at a micrometre scale, or their possible aggregation.

5. Conclusion

Pt/C catalysts have been synthesized by a novel low-temperature plasma method which consists in treating in one step a mixture of a solid metallic precursor and carbon support. The method was used to prepare highly loaded Pt/carbon black cat-alysts designed for PEM fuel cell applications. Various conditions (with or without stirring of the reactants; plasma gas and plasma power; plasma treatment duration; Pt mass loading) have been tested. The Pt/C catalysts, and more specifically the Pt nanopar-ticles, have been characterized by X-ray diffraction, transmission electron microscopy and X-ray photoelectron spectroscopy.

The novel plasma method has been shown very effective for producing materials with the required characteristics for PEM fuel cell electrocatalysis: under a 100 W oxygen plasma with stirring of the reactants during the treatment, Pt nanoparticles with an aver-age diameter of around 3 nm, which are mainly metallic, and quite homogeneously distributed, were deposited on the carbon support. The same characteristics can be obtained up to a Pt loading of at least 40 wt%. Moreover the Pt yield of the method is of around 75%.

A mechanism for the formation of the Pt nanoparticles during the plasma treatment has been proposed: (i) the metallic precur-sor is thermally decomposed; (ii) some oxygenated surface groups or structural defects are formed at the surface of the carbon black powder; (iii) these surface defects act as anchoring sites for the nucleation of Pt nanoparticles. The decomposition of the metallic precursor mainly depends on the power of the plasma discharge whereas the formation of the surface anchoring sites depends on the stirring of the reactants and on the nature of the plasma gas.

Acknowledgements

References

[1] G.W. Crabtree, M.S. Dresselhaus, MRS Bulletin 33 (2008) 421–428.
[2] F. Maillard, P.E.R. Simonov, E.R. Savinova, in: P. Serp, J.L. Figueiredo (Eds.), Carbon Materials for Catalysis, John Wiley & Sons, Inc., New York, 2009, pp. 429–480.
[3] H.A. Gasteiger, S.S. Kocha, B. Sompalli, F.T. Wagner, Applied Catalysis B: Envi-ronmental 56 (2005) 9–35.
[4] M. Watanabe, H. Sei, P. Stonehart, Journal of Electroanalytical Chemistry and Interfacial Electrochemistry 261 (1989) 375–387.
[5] Y. Bultel, P. Ozil, R. Durand, Journal of Applied Electrochemistry 29 (1999) 1025–1033.
[6] N. Job, M. Chatenet, S. Berthon-Fabry, S. Hermans, F. Maillard, Journal of Power Sources 240 (2013) 294–305.
[7] C. Bock, H. Halvorsen, B. MacDougall, in: J. Zhang (Ed.), PEM Fuel Cell Electrocat-alysts and Catalyst Layers: Fundamentals and Applications, Springer, London, 2008, pp. 447–486.
[8] E. Antolini, Journal of Materials Science 38 (2003) 2995–3005.
[9] N. Job, S. Lambert, M. Chatenet, C.J. Gommes, F. Maillard, S. Berthon-Fabry, J.R. Regalbuto, J.-P. Pirard, Catalysis Today 150 (2010) 119–127.
[10] N. Job, J. Marie, S. Lambert, S. Berthon-Fabry, P. Achard, Energy Conversion and Management 49 (2008) 2461–2470.
[11] H. Perez, A. Morin, L. Akrour, C. Cremona, B. Baret, J. Haccoun, S. Escribano, A. Etcheberry, Electrochimica Acta 55 (2010) 2358–2362.
[12] M. Miyake, T. Ueda, T. Hirato, Journal of the Electrochemical Society 158 (2011) D590–D593.
[13] M. Cavarroc, A. Ennadjaoui, M. Mougenot, P. Brault, R. Escalier, Y. Tessier, J. Durand, S. Roualdès, T. Sauvage, C. Coutanceau, Electrochemistry Communica-tions 11 (2009) 859–861.
[14] J. Goswami, C.G. Wang, W. Cao, S.K. Dey, Chemical Vapor Deposition 9 (2003) 213–220.
[15] J.-J. Pireaux, F. Reniers, J. Guillot, M. Gulas, N. Claessens, A. Batan, A. Mansour, Method for depositing nanoparticles on substrates, 2010, WO/2012/028695 A2.
[16] P. Scherrer, Nachrichten von der Gesellschaft Wissensch. zu Göttingen 26 (1918) 98.
[17] N. Job, M.F.R. Pereira, S. Lambert, A. Cabiac, G. Delahay, J.-F. Colomer, J. Marien, J.L. Figueiredo, J.-P. Pirard, Journal of Catalysis 240 (2006) 160–171.
[18] D.A. Shirley, Physical Review B 5 (1972) 4709–4714.
[19] A. Felten, C. Bittencourt, J.J. Pireaux, G. Van Lier, J.C. Charlier, Journal of Applied Physics 98 (2005) 074308.
[20] R. Ionescu, E.H. Espinosa, E. Sotter, E. Llobet, X. Vilanova, X. Correig, A. Fel-ten, C. Bittencourt, G.V. Lier, J.C. Charlier, J.J. Pireaux, Sensors and Actuators B: Chemical 113 (2006) 36–46.
[21] D.-Q. Yang, E. Sacher, Chemistry of Materials 18 (2006) 1811–1816.
[22] M.J. Larsen, E.M. Skou, Journal of Power Sources 202 (2012) 35–46.
[23] J. Croy, S. Mostafa, H. Heinrich, B. Cuenya, Catalysis Letters 131 (2009) 21–32.
[24] XPS Database, Measurement Services Division of National Institute of Standards and Technology, <http://srdata.nist.gov/xps/selEnergyType.aspx> (Accessed October 2012).
[25] Crystallographic and crystallochemical database for minerals and their struc-tural analogues, Institute of Experimental Mineralogy of Russian Academy of Sciences, <http://database.iem.ac.ru/mincryst/index.php> (accessed October 2012).
[26] G. Bergeret, P. Gallezot, in: G. Ertl, H. Knözinger, F. Schüth, J. Weitkamp (Eds.), Handbook of Heterogeneous Catalysis, Wiley-VCH, Weinheim, 2008, pp. 738–765.
[27] A. Fridman, Plasma Chemistry, Cambridge University Press, New York, 2008.
[28] S. Hermans, V. Bruyr, M. Devillers, Journal of Materials Chemistry 22 (2012) 14479–14486.

[29] S. Hermans, C. Diverchy, O. Demoulin, V. Dubois, E.M. Gaigneaux, M. Devillers, Journal of Catalysis 243 (2006) 239–251.

[30] C. Bittencourt, M. Hecq, A. Felten, J.J. Pireaux, J. Ghijsen, M.P. Felicissimo, P. Rudolf, W. Drube, X. Ke, G. Van Tendeloo, Chemical Physics Letters 462 (2008) 260–264.

[31] C. Kuhrt, M. Harsdorff, Surface Science 245 (1991) 173–179.

[32] P. Marcus, C. Hinnen, Surface Science 392 (1997) 134–142.

[33] G.K. Wertheim, S.B. DiCenzo, Physical Review B 37 (1988) 844–847.

[34] G.K. Wertheim, S.B. DiCenzo, S.E. Youngquist, Physical Review Letters 51 (1983) 2310–2313.

[35] L. Chen, A. Yelon, E. Sacher, The Journal of Physical Chemistry C 115 (2011) 7896–7905.

[36] G. Zhang, D. Yang, E. Sacher, Journal of Physical Chemistry C 111 (2006) 565–570.